Design of Structures That Adapt to Loads through Large Shape Changes

Arka P. Reksowardojo[1]; Gennaro Senatore[2]; and Ian F. C. Smith, F.ASCE[3]

Abstract: Adaptive structures can modify their geometry and internal forces through sensing and mechanical actuation in order to maintain optimal performance under changing actions. Previous work has shown that well-conceived adaptive design strategies achieve substantial whole-life energy savings compared with traditional passive designs. The whole-life energy comprises an embodied part in the material and an operational part for structural adaptation. Structural adaptation through controlled large shape changes allows a significant stress redistribution so that the design is not governed by extreme loads with long return periods. This way, material utilization is maximized, and thus embodied energy is reduced. This paper presents a new design process for adaptive structures based on geometry and member sizing optimization in combination with actuator placement optimization. This method consists of two parts: (1) geometry and sizing optimization through sequential quadratic programming is carried out to obtain shapes that are optimal for each load case; and (2) a formulation based on stochastic search and the nonlinear force method (NFM) is employed to obtain an optimal actuator layout and commands to control the structure into the target shapes obtained from Part 1. A case study of a planar statically indeterminate truss is presented. Numerical results show that 17% and 37% embodied energy savings are achieved with respect to an identical active structure designed to adapt through small shape changes and to a weight-optimized passive structure, respectively. The combinatorial task of optimal actuator placement is carried out efficiently. The method formulated in this work produces actuator layouts that enable accurate geometric nonlinear shape control under quasi-static loading through a low number of actuators compared to the number of members of the structure. **DOI: [10.1061/(ASCE)ST.1943-541X.0002604](https://doi.org/10.1061/(ASCE)ST.1943-541X.0002604).** © *2020 American Society of Civil Engineers.*

Author keywords: Adaptive structures; Shape optimization; Shape control; Actuator layout optimization; Nonlinear force method; Geometric nonlinear.

Introduction

The construction industry is a major contributor to the global energy demand ([EEA 2010](#)) and a major consumer of mined raw materials ([Straube 2006](#)). For this reason, it is becoming important to design and construct structures taking into account energy and material efficiency throughout their life cycle. Civil structures are generally designed to meet strength and deformation requirements under worst load case combinations, including long-return-period events such as earthquakes and strong winds. As a result, the majority of civil structures are overdesigned for most of their service life. Previous work ([Senatore et al. 2019](#)) has shown that adaptation to loading is a potential solution to substantially reduce structures energetic impacts. Adaptive structures are equipped with sensors and actuators to control the internal forces and external geometry

[1]Ph.D. Student, Applied Computing and Mechanics Laboratory, School of Architecture, Civil and Environmental Engineering, Swiss Federal Institute of Technology, Lausanne CH-1015, Switzerland. ORCID: https://orcid.org/0000-0002-5626-430X. Email: arka.reksowardojo@epfl.ch

[2]Scientist, Applied Computing and Mechanics Laboratory, School of Architecture, Civil and Environmental Engineering, Swiss Federal Institute of Technology, Lausanne CH-1015, Switzerland (corresponding author). ORCID: https://orcid.org/0000-0001-7418-9713. Email: gennaro.senatore@epfl.ch

[3]Professor, Applied Computing and Mechanics Laboratory, School of Architecture, Civil and Environmental Engineering, Swiss Federal Institute of Technology, Lausanne CH-1015, Switzerland. Email: ian.smith@epfl.ch

in order to achieve optimal performance in response to loads. The ability to adapt to changing loads enables a structure to operate closer to design limits during service.

Extensive studies have been made in active vibration control ([Soong and Cimellaro 2009](#); [Soong 1988](#)). One of the first full-scale implementations was tested in the late 1980s in Japan on a prototype building ([Reinhorn et al. 1993](#)) and on a fully operating commercial building ([Kobori and Kamagata 1991](#)). In both implementations, active control was successfully implemented to compensate for excessive vibrations caused by ground motion and strong winds. However, adoption of adaptive designs has been slow due to control system reliability and robustness issues ([Spencer and Nagarajaiah 2003](#)), as well as to a high initial cost. As extreme excitations typically have long return periods, the uncertainty related to long-term reliability of control systems poses a risk ([Shea et al. 2002](#); [Nakajima et al. 2012](#)). However, if structural adaptation is employed to meet serviceability requirements, long-term reliability of sensors and actuators are of less concern than when primary control objectives are associated with ultimate limit state requirements ([Shea et al. 2002](#); [Connor 2002](#)).

Sobek and Teuffel ([2001](#)) and Teuffel ([2004](#)) showed that force and shape control can be employed to homogenize the stress in pin-jointed structures such that the effect of external loading is reduced. This way it was possible to achieve substantial material mass savings compared to a passive design. However, such savings were achieved at a cost of energy required to operate the adaptive system. Senatore et al. ([2011](#), [2019](#)) formulated a new integrated structure-control method to synthesize adaptive structures through minimization of the whole-life energy, which comprises a part embodied in the material and an operational part for adaptation. If actuation is only employed against rarely occurring loads, a substantial

reduction of material embodied energy can be achieved at a small cost of operational energy (Senatore et al. 2019). Numerical simulations (Senatore et al. 2018a, b) and experimental testing (Senatore et al. 2018c) showed that energy savings up to 70% can be gained by adaptive designs for slender configurations including tall buildings, bridges, and self-supporting roof systems of complex layout. The formulation given by Senatore et al. (2019) is based on the assumption of small deformations, and thus control is limited to small shape changes.

Large geometric reconfigurations have been achieved by deployable structures whose motion is based on component mechanisms with defined kinematics (e.g., scissor systems) (Pellegrino 2001). Deployable structures have been applied in civil engineering mostly as large-scale retractable roof systems (Gantes et al. 1989; Akgün et al. 2011). However, these structures usually cannot bear loads until the deployed state is reached. Shape control of load-bearing tensegrity structures has been investigated (Rhode-Barbarigos et al. 2012; Adam and Smith 2008). Due to the usually complex kinematics of tensegrity structures that causes geometric nonlinearity, adaptation and deployment were implemented combining physics-based models with machine learning and stochastic optimization (Veuve et al. 2015; Sychterz and Smith 2018).

Shape optimization has been subject of extensive research. Depending on the external load, it was shown that optimal shapes resemble arches (Wang et al. 2002; Querin 1997), catenaries, and lenticular configurations (Gil and Andreu 2001). Geometry optimization of a simply supported planar truss under uniformly distributed load was shown to be 70% lighter than the initial flat configuration of constant depth (Gil and Andreu 2001; Wang et al. 2002). In Pedersen and Nielsen (2003), a spatial truss of variable depth was further improved through shape optimization. Although the optimal solution retained the features of the initial shape, small adjustments of the truss depth resulted in 35% mass savings with respect to the initial configuration. Existing geometry optimization techniques aim to obtain one efficient shape that is a best fit under multiple load cases. Instead, if the structure adapts to loading by a change of geometry, there could be as many optimal shapes as the design loads are and thus structural efficiency could be improved.

Designing an actuation system for structural control is a twofold task (Soong and Cimellaro 2009): (1) obtain appropriate commands to control the structure; and (2) obtain an optimal actuator placement that allows to control the structure with minimum effort. Integrated structure-control design can produce an optimal actuator placement to minimize control effort (Soong and Manolis 1987; Skelton and Sultan 1997). For a reticular structure, optimal actuator placement is of a combinatorial nature because it involves placing actuators within a set of available locations (i.e., the structural elements). This makes integrated design of structure–control system a challenging task.

In the context of vibration control, integrated designs have been achieved through minimizing control effort or other cost functions (e.g., the linear-quadratic regulator). Simultaneous optimization of structural parameters and control, including the actuator placement, has been implemented using stochastic optimization aided by ad hoc heuristics (Manning 1991; Begg and Liu 2000), resulting in efficient designs albeit only exploring a fraction of a large solution domain. In Korkmaz et al. (2012), shape control of a tensegrity structure was investigated. Actuator placement was implemented through a multiobjective optimization for damage tolerance subject to strength and serviceability requirements. The dynamic relaxation (DR) method was employed to predict shape changes given a set of actuator commands. DR is an efficient method to handle geometric nonlinearity (Sauve 1995; Senatore and Piker 2015). However, DR does not offer an efficient formulation to solve the inverse problem, which is to the obtain control commands given a target shape.

In Senatore et al. (2019), the actuator locations were determined through a measure of efficacy that evaluates the contribution of a structural element toward the required force and shape control. Deformations caused by initial imperfections (eigenstrain) were interpreted to be caused by actuator length changes. This idea made it possible to formulate a computationally efficient routine based on the integrated force method (IFM) (Patnaik et al. 2004) to obtain optimal actuator layouts for structures that adapt to loads through small shape changes (small deformation assumption). Yuan et al. (2016) presented a formulation called nonlinear force method, which was employed to obtain suitable actuation commands to control large shape changes. Computation of actuator commands was formulated as an iterative processs, which generally requires a low number of iterations to achieve convergence. However, in Yuan et al. (2016) no process was formulated to obtain the actuator placement, which was determined a priori.

Outline

This paper presents a new method to design adaptive structures capable of large and reversible shape changes achieved through actuation. This work extends the formulation given in Senatore et al. (2019) in that the structure is designed to adapt to loads through large shape changes, i.e., small strains but large displacements assumption. Shape adaptation does not rely on mechanisms with defined kinematics (e.g., scissor systems). In the event of a strong loading event, a change of shape takes place to homogenize stresses thus minimizing the maximum stress governing the design. Because large shape changes induce geometrical nonlinearity, this work is not based on a small deformation assumption. A set of target shapes that counteract the effect of peak loads are first obtained through geometry and sizing optimization. A method is formulated to obtain a suitable actuator layout in order to control the structure into the target shapes. This method is a combination of stochastic search and a nonlinear force method (Yuan et al. 2016) in a nested optimization scheme.

An application of this design process on a planar truss is presented. The solution produced by this process is benchmarked against an adaptive structure limited to small shape changes obtained using the formulation given by Senatore et al. (2019) and a weight-optimized passive structure of identical topology.

Design Method

The design method presented in this paper is implemented for reticular structures. The active elements are assumed to be linear actuators that are fitted within some of the structure elements. The design method consists of two parts:
1. Optimization of the geometry and internal forces for each load case as well as optimization of the element cross-sectional areas in order to minimize the structure embodied energy.
2. Optimal actuator placement to control the structure into the target optimal shapes obtained in Part 1.
   Fig. 1 shows a flowchart of the design process.

Shape and Internal Load-Path Optimization

The structure is designed to have an optimal shape and internal load-path against each load case. This process, denoted by χ, is a mapping between external load $\mathbf{p}$ and target shapes $\mathbf{d}^t$ as well as internal forces $\mathbf{f}^t$ (the superscript t stands for target) that are optimized to maximize material utilization
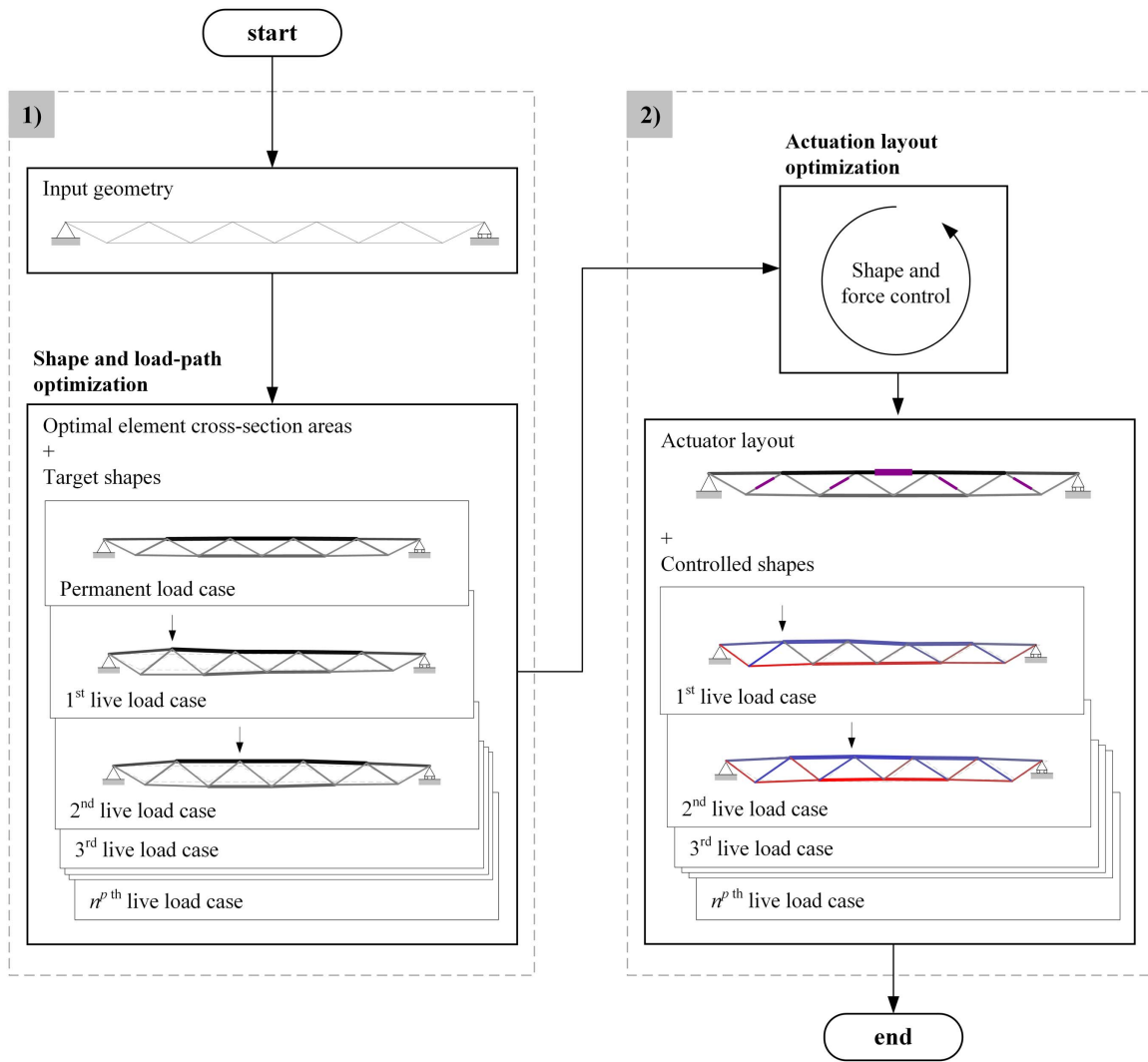
Fig. 1. Design method flowchart.

$$\chi : \mathbf{p}_j \rightarrow (\mathbf{f}_j^t, \mathbf{d}_j^t) \quad \forall\; j = 0, 1, \ldots, n^p,$$

$$\mathbf{p}_j \mapsto \mathbf{f}_j^t(\mathbf{p}_j),$$

$$\mathbf{p}_j \mapsto \mathbf{d}_j^t(\mathbf{p}_j) \tag{1}$$

Internal load-path and internal forces have the same meaning in this paper. The main inputs are the structural topology, i.e., a set of n^n nodes connected by n^e elements in two or three-dimensions and support conditions. Because the structure is reticular, there are $n^d = n^n \cdot dim$ degrees of freedom (DOF), where dim is either 2 or 3. The controlled degrees of freedom are those allowed to vary during shape optimization and will be controlled through actuation. The initial shape of the structure (i.e., initial node coordinates) is defined as $\mathbf{d}^{\text{input}} \in \mathbb{R}^{n^d}$. The design variables are the element cross-sectional areas $\boldsymbol{\alpha} \in \mathbb{R}^{n^e}$, internal forces $\mathbf{f} \in \mathbb{R}^{2 \cdot n^e}$, and nodal positions $\mathbf{d}^t \in \mathbb{R}^{n^d}$

$$\mathbf{x} = [\boldsymbol{\alpha} \quad \mathbf{f}_0 \quad \cdots \quad \mathbf{f}_j \quad \cdots \quad \mathbf{f}_{n^p} \quad \mathbf{d}_0^t \quad \cdots \quad \mathbf{d}_j^t \quad \cdots \quad \mathbf{d}_{n^p}^t]^T \tag{2}$$

where index i refers to the ith element; j refers to the jth load case; and n^p is the total number of load cases. There are n^p vectors of nodal positions $\mathbf{d}^t$ and internal forces $\mathbf{f}$, to be achieved through control. There is only one vector of element cross-sectional areas $\boldsymbol{\alpha}$, which remains constant during control. The superscript or subscript

0 indicates the case where only permanent load is applied (i.e., no live load).

Following the simultaneous analysis and design approach (SAND), the internal forces are treated as variables by adding extra equality constraints to enforce equilibrium, therefore avoiding a direct matrix inversion (Haftka 1985).The internal forces $\mathbf{f}_j$ include two vectors

$$\mathbf{f}_j = [\mathbf{f}_j^t \quad \mathbf{f}_j^0]^T \tag{3}$$

where $\mathbf{f}_j^t$ = forces in equilibrium with the external load through a shape change $\mathbf{d}_j^t$; and $\mathbf{f}_j^0$ = forces in equilibrium with the external load without shape control and computed on $\mathbf{d}_0^t$ the optimal shape under permanent load only.

The structure is assumed to be built with shape $\mathbf{d}_0^t$ because it is the most efficient geometry in the absence of live load. Including the forces $\mathbf{f}_j^0$ within the design variables produces structures that are fail-safe without the contribution of the active system. In the event of control system failure or power outage and simultaneous occurrence of the worst load case, load-carrying capacity is not exceeded.

The objective of this part of the design process is minimization of the energy embodied in the material for extraction and manufacturing subject to force equilibrium and ultimate limit state (ULS) constraints. The formulation is given as follows:

$$\min_{\mathbf{x}} \sum_{i=1}^{n^e} g_i \alpha_i l_{i0} \rho_i, \quad \text{s.t.} \tag{4}$$

$$\mathbf{A}_j \mathbf{f}_j^t = \mathbf{p}_j \tag{5}$$

$$\begin{bmatrix} \mathbf{A}_0 \\ (\mathbf{W}_s)^T \mathbf{G} \end{bmatrix} \mathbf{f}_j^0 = \begin{Bmatrix} \mathbf{p}_j^0 \\ \mathbf{0} \end{Bmatrix} \tag{6}$$

$$f_{ij}^t \le \sigma_i^+ \alpha_i; \qquad f_{ij}^t \ge \max\left(\sigma_i^- \alpha_i, -\frac{\pi^2 EI_i}{l_{ij}^2}\right) \tag{7}$$

$$f_{ij}^0 \le \sigma_i^+ \alpha_i; \qquad f_{ij}^0 \ge \max\left(\sigma_i^- \alpha_i, -\frac{\pi^2 EI_i}{l_{i0}^2}\right) \tag{8}$$

$$\mathbf{d}^l \le \mathbf{d}^t \le \mathbf{d}^u \tag{9}$$

$$\boldsymbol{\alpha}^l \le \boldsymbol{\alpha} \tag{10}$$

The objective function in Eq. (4) is the embodied energy where g_i is the material energy intensity (Hammond and Jones 2008), α_i the cross-sectional area and ρ_i the material density of the ith element. The term l_{ij} is the length of the ith element for the jth load case.

In Eq. (5) $\mathbf{A}_j \in \mathbb{R}^{n^d \times n^e}$, $\mathbf{f}_j$ and $\mathbf{p}_j$ are the equilibrium matrix, internal forces, and external load for the jth load case. The equilibrium matrix $\mathbf{A}$ is a concatenation of direction cosine vectors $\boldsymbol{\theta}_i$, i.e., the cosines of the angles made by the ith element with respect to the global coordinate axes

$$\mathbf{A} = [\boldsymbol{\theta}_1 \quad \cdots \quad \boldsymbol{\theta}_i \quad \cdots \quad \boldsymbol{\theta}_{n^e}] \tag{11}$$

where the direction cosine vector for the ith element is

$$\boldsymbol{\theta}_i = \frac{\sqrt{2}}{\|\mathbf{C}_i \mathbf{d}^t\|_2} \mathbf{C}_i \mathbf{d}^t \tag{12}$$

$\mathbf{C}_i \in \mathbb{R}^{n^d \times n^d}$ = connectivity matrix of the ith element, which contains all zero entries except for the rows corresponding to the degrees of freedom of the ith element ends, which are set to 1 and -1 (Descamps 2014; Achtziger 2007). Because large shape changes are considered, the equilibrium matrix $\mathbf{A}_j$ and the element length l_{ij} depend on of the nodal positions $\mathbf{d}_j^t$. Note that for clarity the function notation is omitted, e.g., $\mathbf{A}_j$ instead of $\mathbf{A}_j(\mathbf{d}_j^t)$.

In Eq. (6), $\mathbf{G} \in \mathbb{R}^{n^e \times n^e}$ and $\mathbf{W}_s \in \mathbb{R}^{n^e \times r}$ are the element flexibility matrix and the null space of $\mathbf{A}_0$ computed for $\mathbf{d}_0^t$, i.e., the target shape under permanent load only. The rows of $\mathbf{W}_s$ are the r states of self-stress, where r is the degree of static indeterminacy [see section "Computation of Control Commands Given Target Internal Forces and Shape (ϕ^{-1})"]. The $\mathbf{p}_j^0$ is the external load considered in the fail-safe measure for the jth load case. Eq. (6) is the governing equation of the integrated force method (Patnaik et al. 2004). A detailed formulation of the IFM for design and optimization of adaptive structures is given in Senatore et al. (2019).

The primary difference between $\mathbf{f}^0$ and $\mathbf{f}^t$ is that the former are compatible forces while the latter are not. Eq. (6) includes geometric compatibility between element deformations and nodal displacements by adding r equations of compatibility to force equilibrium, i.e., the product of self-stress by element flexibility $(\mathbf{W}_s)^T \mathbf{G}$. The internal forces $\mathbf{f}^0$ must be compatible so that element capacity is not exceeded in case of control system failure and simultaneous occurrence of the design load. Note that no deflection limit is considered at this stage.

However, geometric compatibility is not included in Eq. (5), and therefore the target internal forces $\mathbf{f}^t$ and shapes $\mathbf{d}^t$ are not compatible. In other words, the nodal positions obtained through this process are not identical to those that result by calculating element deformations under the external load. Geometric compatibility is a nonlinear constraint that is often ignored in structural optimization because it might cause convergence issues (Descamps 2014). For a passive structure, this omission results in a postdesign phase to produce a structure that satisfies serviceability limit state (SLS) criteria, for example, deflection limits under loading. Conversely, as already shown in Senatore et al. (2019), disaggregation of equilibrium and geometric compatibility is a key aspect for designing an efficient adaptive structure. If the structure is adaptive, it can be designed to satisfy ULS criteria passively while SLS (deflections) criteria are met through controlled shape changes. Similarly, in this work, the active system is employed to control the structure into target geometrical shapes that are structurally efficient for each load case.

Eq. (7) constrains the internal forces $\mathbf{f}^t$ within required limits for tension and compression as well as for element buckling. The same applies to Eq. (8) for the internal forces $\mathbf{f}^0$. The second moment of area I_i is a function of the cross-sectional area α_i. E, σ^+ and σ^- are the Young's modulus, admissible tensile, and compressive stress, respectively.

Eq. (9) defines upper and lower limits for $\mathbf{d}^t$ to bound the nodal positions in relative proximity to the input shape $\mathbf{d}^{\text{input}}$. This is to ensure control feasibility by avoiding extremely large shape changes and to ensure, albeit approximately, that the maximum actuator stroke is not exceeded. Because topology optimization is not of interest in this work, a lower limit for $\boldsymbol{\alpha}$ is also defined in Eq. (10) to avoid vanishing elements, i.e., elements with infinitely small cross section. The search space of the optimization problem stated in Eqs. (4)–(10) is continuous but not convex because the nodal coordinates are part of the design variables and due to the element buckling constraint (Schwarz et al. 2018). This problem was solved through sequential quadratic programming (SQP) (Boogs and Tolle 1995). Because the structure is assumed to be built with shape $\mathbf{d}_0^t$, the active system will control the structure from $\mathbf{d}_0^t$ rather than $\mathbf{d}^{\text{input}}$. For this reason, target force and target shape difference are defined with respect to $\mathbf{d}_0^t$ as

$$\begin{aligned} \Delta \mathbf{f}_j^t &:= \mathbf{f}_j^t - \mathbf{f}_j^0 \\ \Delta \mathbf{d}_j^t &:= \mathbf{d}_j^t - \mathbf{d}_j^0 \end{aligned} \quad \forall \; j = 1, \ldots, n^p \tag{13}$$

where $\mathbf{f}_j^0$ and $\mathbf{d}_j^0$ = noncontrolled internal forces and displacements caused by the jth load case applied on $\mathbf{d}_0^t$. For the sake of clarity, $\mathbf{f}_j^0$ is a design variable of χ [Eqs. (3) and (6)]. However, $\mathbf{d}_j^0$ is a state variable computed through structural analysis from $\mathbf{f}_j^0$.

Actuation Layout Optimization

The second step of the design process is to obtain an actuator layout (i.e., placement) that is optimal for controlling the structure into the target shapes obtained through χ. Due to the combinatorial nature of optimal actuator placement combined with geometric nonlinearity caused by shape control, this process is carried out using a global search method called constrained simulated annealing (CSA) (Wah and Wang 1999). To evaluate the efficacy of a candidate actuator layout, force and shape control are carried out using the process explained in section "Quasi-Static, Nonlinear Geometric Shape and Force Control." Force equilibrium, stress constraints, and geometric compatibility must be considered at this stage.

The objective is to maximize the similarity between shapes controlled through actuation and the target shapes subject to

USL constraints. The similarity of controlled shapes with target ones has to be assessed for each load case and combined into one scalar, which is a measure of the control efficacy of a candidate actuator layout. A similarity measure based on Euclidean distance cannot be used because in the absence of a common reference shape, it is difficult to quantify the degree of similarity across multiple load cases. For instance, a similarity measure based on the squared difference between the nodal positions of controlled and target shapes cannot be normalized across different load cases and thus it might introduce bias. For this reason, shape similarity is evaluated using the Tanimoto index (Tanimoto 1958), a similarity criterion so far employed in machine learning and data mining applications (Doan et al. 2004; Bajusz et al. 2015)

$$Q = \frac{1}{n^p} \sum_{j=1}^{n^p} \frac{(\Delta \mathbf{d}_j^c)^T \Delta \mathbf{d}_j^t}{(\Delta \mathbf{d}_j^c)^T \Delta \mathbf{d}_j^c + (\Delta \mathbf{d}_j^t)^T \Delta \mathbf{d}_j^t - (\Delta \mathbf{d}_j^c)^T \Delta \mathbf{d}_j^t} \quad (14)$$

This similarity criterion measures the difference between two vectors in terms of directions and magnitude, which in this context represent shape features and node positions, respectively. The $\Delta \mathbf{d}^t$ is the nodal displacement vector to move from the deformed shape to the target shape. Similarly, $\Delta \mathbf{d}^c$ is the nodal displacement vector to move from deformed shape to the shape controlled through actuation [obtained from ϕ; see section "Computation of Internal Forces and Shape Given Control Commands (ϕ)"]. Eq. (14) returns a value between 0 and 1. The closer the value to 1 the closer the control shape is to the target shape across n^p load cases. The actuator layout is obtained as the optimal solution of the following problem:

$$\min_{\mathbf{y}} 1 - Q, \quad \text{s.t.} \quad (15)$$

$$f_{ij}^c \leq \sigma_i^+ \alpha_i; \qquad f_{ij}^c \geq \max\left(\sigma_i^- \alpha_i, -\frac{\pi^2 EI_i}{l_{ij}^2}\right) \quad (16)$$

where $\mathbf{y} \in \mathbb{Z}^{n^{act}}$ = vector of element indices that are assigned as active elements; and n^{act} = number of actuators, which is assigned a priori. Ultimate limit state (ULS) is applied as a constraint. The problem stated in Eqs. (15) and (16) is combinatorial and not continuous because the design variable $\mathbf{y}$ consists of only integers. The task of selecting n^{act} actuators from n^e element locations has a search space size of

$$\frac{n^e!}{n^{act}!(n^e - n^{act})!} \quad (17)$$

When the number of structural elements is large, a full enumeration is computationally impossible. A stochastic search based on simulated annealing method (SA) (Kirkpatrick et al. 1983; Cerny 1985) is formulated. SA, which has found applications in various engineering domains (Onoda and Hanawa 1992; Arora et al. 1995; Reddy and Cagan 1995), mimics the cooling process of molten metals through metallurgical annealing. In this physical process, as the temperature decreases, particles arrange into a low energy state. In the context of numerical optimization, a low-energy state corresponds to an optimal solution. In SA, a parameter T steers the search within the neighborhood of candidate solutions. A neighborhood structure defines how to update the current solution $\mathbf{y}$ to its neighbor $\mathbf{y}'$ within the solution space. While the value of T is high, a neighbor is likely to be accepted, regardless of its fitness. As T reduces, neighbor solutions with a lower fitness score are more likely to be rejected; thus, the search is intensified in the region of good solutions (Metropolis et al. 1953).

In constrained simulated annealing (Wah and Wang 1999), an auxiliary design variable, the penalty factor γ is introduced to penalize candidate solutions that violate the constraints. The neighborhood structure of γ is different to that of $\mathbf{y}$, therefore the search is performed in a combined solution + penalty space. The range for γ can be set to an arbitrarily high value, or to the average value of admissible stress and buckling constraint violations for a large number of randomly generated solutions. The value of the penalty increases as T decreases. While T is high, a solution is likely to be accepted, even if the solution violates the constraints. To account for the penalty factor, the problem stated in Eq. (15) is rewritten

$$\min_{\mathbf{y}} J \quad (18)$$

where J = joint objective function, defined as follows:

$$J = 1 - Q + \gamma \quad (19)$$

The actuator layout $\mathbf{y}$ is updated using a measure of efficacy to assess how each element contributes to attain the target shapes by changing its length. The efficacy measure is inspired by a method presented by Senatore et al. (2019), which was formulated based on the assumption of small deformations. When geometrical nonlinearity is considered, the effect of multiple actuators is not equivalent to the superposition of the individual effects. Therefore, in this work, the measure of efficacy is not used directly for selecting actuator locations. It is instead employed as a heuristic to introduce bias in the search process by giving candidate locations with a higher control efficacy, a greater probability to be included in the candidate solution. The efficacy measure is computed in three steps:

1. Assuming all the elements are active, their length changes to control the structure into the target shapes are computed using ϕ^{-1} [see section "Computation of Control Commands Given Target Internal Forces and Shape (ϕ^{-1})"];
2. The response of the structure is evaluated by applying the length change of each element in turn (using ϕ; see section "Computation of Internal Forces and Shape Given Control Commands (ϕ)"] extracted from the control command vector obtained in Step 1; and
3. The control efficacy is measured using the Tanimoto index in Eq. (14) to evaluate the similarity between the target shapes and the shapes caused by the length change of each element in turn.

The process is repeated to compute the control efficacy for each element, which is normalized to form a vector $\mathbf{P} \in \mathbb{R}^{n^e}$

$$\mathbf{P} = \frac{[Q_1 \quad \cdots \quad Q_i \quad \cdots \quad Q_{n^e}]^T}{\sum_{i=1}^{n^e} Q_i} \quad (20)$$

Vector $\mathbf{P}$ can also be thought of as a discrete probability distribution function that is employed to generate a neighbor solution $\mathbf{y}'$. The very first candidate solution $\mathbf{y}^0 \in \mathbb{Z}^{n^{act}}$ is obtained as the topmost n^{act} elements ranked in terms of the efficacy measure $\mathbf{P}$. The generation of next neighbor solutions is obtained by drawing a random integer that is the number of actuator locations to be replaced from a discretized uniform distribution. An actuator location is removed from the current solution through drawing from the reciprocal distribution function $1/\mathbf{P}$. The removed actuator is then replaced through drawing from $\mathbf{P}$, which is reduced after each draw by removing the selected element in order to avoid selecting the same element more than once (i.e., drawing without replacement).

This process is repeated as many times as the number of actuators to be replaced in order to form the new neighbor solution $\mathbf{y}'$, which will be accepted as a candidate solution with the following probability:

$$O^{\mathbf{y}} = \exp\left(-\frac{J(\mathbf{y}', \gamma) - J(\mathbf{y}, \gamma)}{T}\right) \tag{21}$$

When the value of T is high, if $\mathbf{y}'$ is worse than the current solution $\mathbf{y}$ [i.e., $J(\mathbf{y}', \gamma) > J(\mathbf{y}, \gamma)$] it could still be accepted with a high probability, allowing the search to explore more extensively. As T is reduced, the acceptance probability $O^{\mathbf{y}}$ decreases, thereby the search is intensified in the region of good solutions.

The penalty factor γ is updated by generating a neighbor γ' through drawing from a uniform distribution U within the interval of 0 and 1. The updated γ' will be accepted with the following probability:

$$O^{\gamma} = \exp\left(-\frac{J(\mathbf{y}, \gamma) - J(\mathbf{y}, \gamma')}{T}\right) \tag{22}$$

When the value of T is high, if γ' is lower than the current penalty value γ [i.e., $J(\mathbf{y}, \gamma) > J(\mathbf{y}, \gamma')$], it still has a high probability to be accepted. However, as T is reduced, the acceptance probability O^{γ} decreases, thereby the search is intensified in the region of feasible solutions. Over iterations, $\mathbf{y}$ and γ have equal probability to update to a neighbor $\mathbf{y}'$ and γ'. However, within a single iteration they do not update simultaneously.

A cycle contains $n^{temp} \cdot n^{rep}$ iterations. Thus, T is updated n^{temp} times. At the kth update T_k is

$$T_k = -\frac{1}{\log\left(1 - \frac{k}{n^{temp}}\right)} \tag{23}$$

At each T_k, either $\mathbf{y}'$ or γ' are updated n^{rep} times. The number of temperature levels n^{temp} and that of repetitions n^{rep} are assigned so that the product $n^{temp} \cdot n^{rep}$ is sufficiently large relative to the number of variables + number of constraints. Once a cycle is completed, the search is restarted from the best recorded solution. The process is repeated until convergence, i.e., when no better solution can be obtained after consecutive searches. Algorithm 1 summarizes in steps the CSA-based actuator layout search process explained in this section.

Algorithm 1. Pseudocode of the actuator layout search

```
1     set initial layout y←y⁰
2     set initial penalty γ←0
3     for k←1 to n^temp do
4            update T [Eq. (23)]
5            for l←1 to n^rep do
6                   if random number U[0,1] < 0.5 then
7                          generate a neighbor in solution space y'
                          drawing from P [Eq. (20)]
8                          evaluate y' using Eq. (14) with Δd^c obtained
                          through φ⁻¹
9                          if y' is accepted [Eq. (21)] then y←y'
10                  else
11                         generate a neighbor in penalty space
                          γ' = U[0,1]
12                         if γ' is accepted [Eq. (22)] then γ←γ'
13           end for
14    end for
```

Quasi-Static, Nonlinear Geometric Shape and Force Control

During control, the objective is to obtain commands in order to cause internal force and shape changes that best approximate

the target ones (see section "Shape and Internal Load-Path Optimization"). The method described in this section is based on the non-linear force method through a formulation presented in Yuan et al. (2016).

Computation of Internal Forces and Shape Given Control Commands (φ)

The process of computing changes of nodal displacements $\Delta \mathbf{d}^c$ and internal forces $\Delta \mathbf{f}^c$ under the combined effect of the external load $\mathbf{p}$ and a given set of control commands $\Delta \mathbf{l} \in \mathbb{R}^{n^{act}}$ (i.e., actuator length changes) is denoted as ϕ

$$\phi : (\mathbf{p}_j, \Delta \mathbf{l}_j) \rightarrow (\Delta \mathbf{f}_j^c, \Delta \mathbf{d}_j^c) \quad \forall \, j = 1, \ldots, n^p \tag{24}$$

where superscript c stands for controlled via actuation. Both change of shape $\Delta \mathbf{d}^c$ and internal forces $\Delta \mathbf{f}^c$ can be thought of as a function of the external load $\mathbf{p}$ and control commands $\Delta \mathbf{l}$

$$\begin{aligned}(\mathbf{p}_j, \Delta \mathbf{l}) &\mapsto \Delta \mathbf{f}_j^c(\mathbf{p}_j, \Delta \mathbf{l}_j) \\ (\mathbf{p}_j, \Delta \mathbf{l}) &\mapsto \Delta \mathbf{d}_j^c(\mathbf{p}_j, \Delta \mathbf{l}_j)\end{aligned} \quad \forall \, j = 1, \ldots, n^p \tag{25}$$

Because the process is nonlinear, generally ϕ is iterative. The convergence criterion is based on equilibrium between internal forces and external load by reducing the residual forces below a set tolerance. Geometric compatibility between element deformations and nodal displacements is considered. The ϕ can be any method that is able to simulate geometric nonlinear behavior such as the nonlinear force method (Xu and Luo 2009; Yuan et al. 2016), dynamic relaxation (Barnes 1977; Day 1965), and nonlinear stiffness method (Crisfield 1981).

Computation of Control Commands Given Target Internal Forces and Shape (φ⁻¹)

The inverse process to ϕ is to compute actuator commands $\Delta \mathbf{l}$ to control a target force $\Delta \mathbf{f}^t$ and shape $\Delta \mathbf{d}^t$ change

$$\begin{aligned}\phi^{-1} : (\Delta \mathbf{f}_j^t, \Delta \mathbf{d}_j^t) &\rightarrow \Delta \mathbf{l}_j \quad \forall \, j = 1, \ldots, n^p, \\ (\Delta \mathbf{f}_j^t, \Delta \mathbf{d}_j^t) &\mapsto \Delta \mathbf{l}_j(\Delta \mathbf{f}_j^t, \Delta \mathbf{d}_j^t)\end{aligned} \tag{26}$$

where $\Delta \mathbf{l}$ is thought of as a function of target force $\Delta \mathbf{f}^t$ and shape $\Delta \mathbf{d}^t$ changes.

For small deformations, the shape $\mathbf{S}_d \in \mathbb{R}^{n^d \times n^e}$ and force $\mathbf{S}_f \in \mathbb{R}^{n^e \times n^e}$ influence matrices relate element length changes $\Delta \mathbf{l}^e \in \mathbb{R}^{n^e}$ to changes of shape $\Delta \mathbf{d}$ and internal forces $\Delta \mathbf{f}$

$$\Delta \mathbf{f} = \mathbf{S}_f \Delta \mathbf{l}^e \tag{27}$$

$$\Delta \mathbf{d} = \mathbf{S}_d \Delta \mathbf{l}^e \tag{28}$$

$$\mathbf{S}_f = -\mathbf{W}_s (\mathbf{W}_s^T \mathbf{G} \mathbf{W}_s)^{-1} \mathbf{W}_s^T \tag{29}$$

$$\mathbf{S}_d = \mathbf{B}^+ [\mathbf{I} - \mathbf{G} \mathbf{W}_s (\mathbf{W}_s^T \mathbf{G} \mathbf{W}_s)^{-1} \mathbf{W}_s^T] \tag{30}$$

Note that in Eqs. (27) and (28), $\Delta \mathbf{l}^e$ is length change of all the elements that are considered active at this stage. The $\mathbf{B}^+$ is the generalized inverse of the compatibility matrix $\mathbf{B} \in \mathbb{R}^{n^e \times n^d}$ (transpose of the equilibrium matrix $\mathbf{A}$) and $\mathbf{G} \in \mathbb{R}^{n^e \times n^e}$ is the

member flexibility matrix. The matrix $\mathbf{W}_s \in \mathbb{R}^{n^e \times r}$ is obtained by singular value decomposition (SVD) of the equilibrium matrix $\mathbf{A}$

$$\mathbf{A} = \begin{bmatrix} \mathbf{U}_r & \mathbf{U}_q \end{bmatrix} \begin{bmatrix} \mathbf{V}_r & \mathbf{0} \\ \mathbf{0} & \mathbf{0} \end{bmatrix} \begin{bmatrix} \mathbf{W}_r & \mathbf{W}_s \end{bmatrix}^T \qquad (31)$$

The rows of $\mathbf{W}_s$ are the r states of self-stress, where r is the degree of static indeterminacy. Thus, for a statically determinate system $\mathbf{W}_s$ does not exist. Further inspection of Eqs. (29) and (30) shows that for statically determinate systems $\mathbf{S}_d$ can simply be expressed as $\mathbf{B}^{-1}$, while $\mathbf{S}_f$ does not exist. This means for statically determinate structures, the actuator length changes do not directly cause a change of internal forces because the corresponding change of shape is not resisted by passive stiffness. However, due to

geometric nonlinearity, a change of shape caused by the actuator length changes result in a change of forces regardless the degree of static indeterminacy of the structure.

Given an actuator layout, the shape influence matrix is reduced to $\mathbf{S}_d^* \in \mathbb{R}^{n^{cd} \times n^{act}}$, which contains only the rows and columns corresponding to the controlled degrees of freedom n^{cd} and active elements n^{act}, respectively. Similarly, $\mathbf{S}_f^* \in \mathbb{R}^{n^e \times n^{act}}$ is the force influence matrix $\mathbf{S}_f$ whose columns are reduced to contain only those corresponding to the active elements n^{act}. Usually, the number of controlled degrees of freedom is higher than that of the actuators because it is desirable to employ a simple actuation system in order to reduce installation and maintenance costs as well as control complexity. As a result, $\mathbf{S}_d^*$ and $\mathbf{S}_f^*$ are generally rectangular matrices with significantly more rows than columns (i.e., linear system with
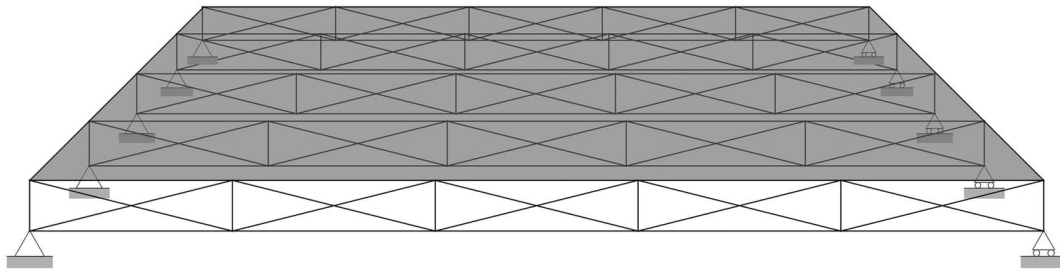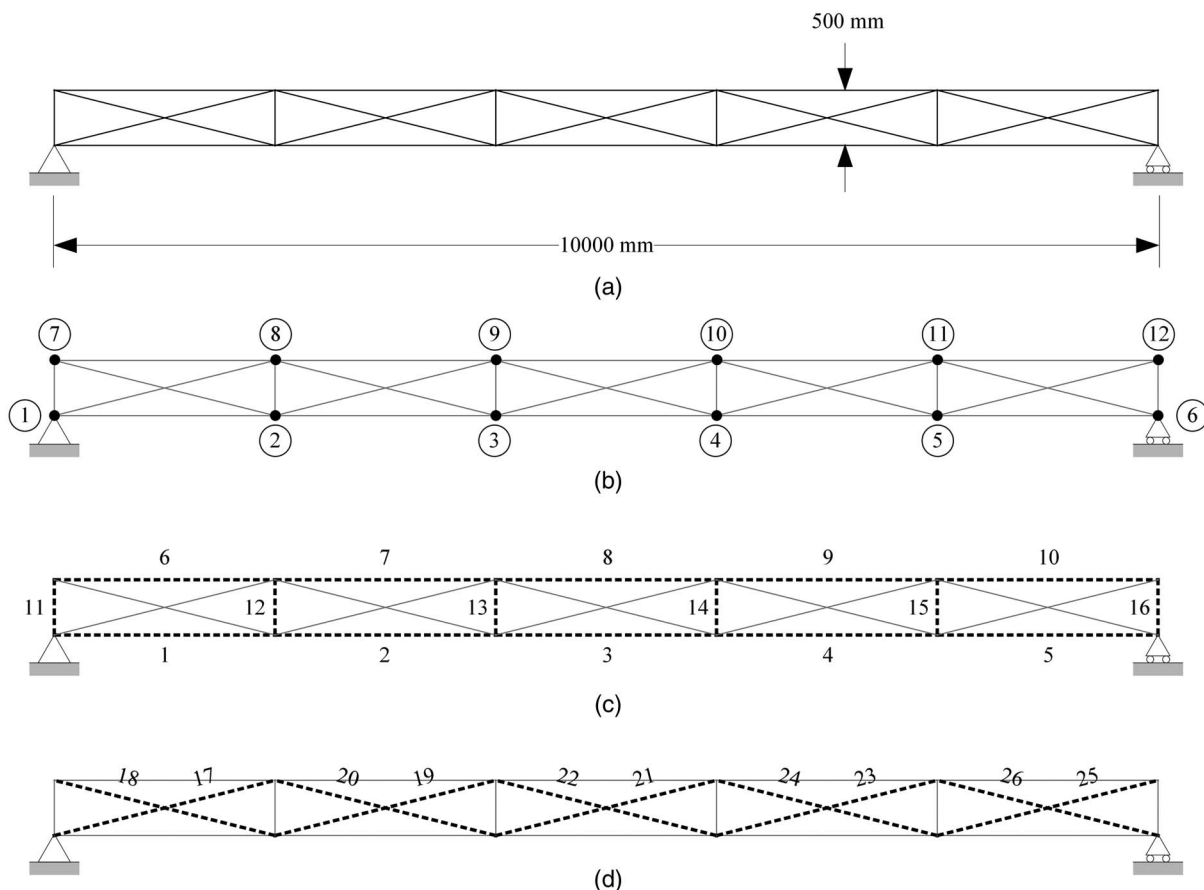

Fig. 2. Roof structure.

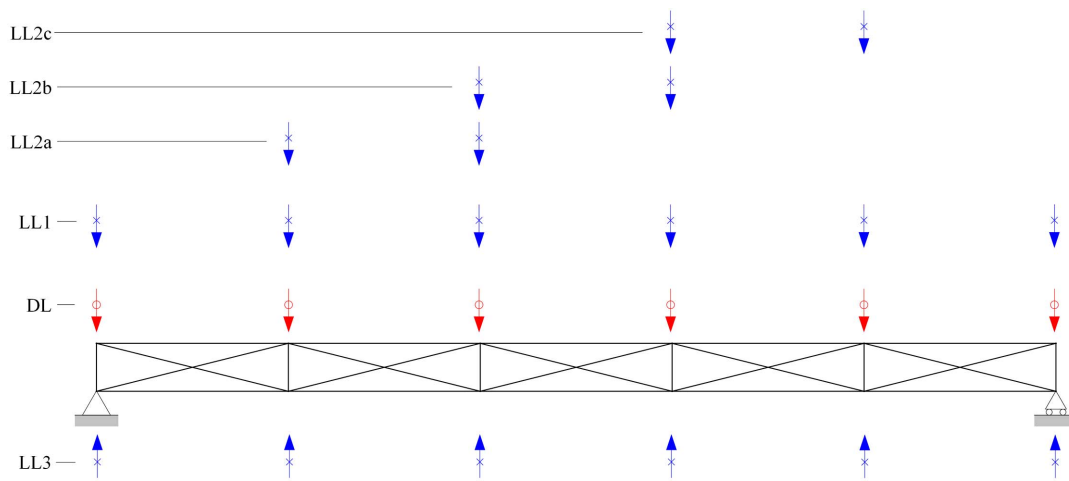**Fig. 3.** (a) Initial geometry; (b) node numbers; and (c and d) element numbers.

Fig. 4. Load cases: Dead load indicated by [○]; and live load indicated by [×].

Table 1. Load combinations

Load case	Load combination
LC0 (permanent load case)	$1.35\,(\mathrm{SW} + \mathrm{DL})$
LC1 to LC4	$1.35\,(\mathrm{SW} + \mathrm{DL}) + 1.5\,(\mathrm{LL1\ to\ LL2})$
LC5	$0.9\,(\mathrm{SW} + \mathrm{DL}) + 1.5\ \mathrm{LL3}$

more equations than unknowns). Therefore, the control commands $\Delta \mathbf{l} \in \mathbb{R}^{n^{act}}$ to reach the target shapes and internal forces are obtained through an approximate solution via least square optimization subject to ULS constraints

$$\min_{\Delta \mathbf{l}} \left\| \mathbf{S} \cdot \Delta \mathbf{l} - \left\{ \begin{array}{c} \Delta \mathbf{d}^t \\ \Delta \mathbf{f}^t \\ \mathbf{0} \end{array} \right\} \right\|_2 \quad \text{s.t.} \tag{32}$$

$$f_i^c \leq \sigma_i^+ \alpha_i; \qquad f_i^c \geq \max\left(\sigma_i^- \alpha_i, -\frac{\pi^2 E I_i}{l_i^2} \right) \tag{33}$$

where the term $\mathbf{S}$ is

$$\mathbf{S} = [\,\mathbf{S}_d^* \quad \mathbf{S}_f^* \quad \mathbf{I}\,]^T \tag{34}$$

The term $\mathbf{I}$ is the identity matrix of size n^{act}, which is introduced to obtain the minimum norm $\Delta \mathbf{l}$ in order to avoid large actuator length changes which might cause numerical instability and might also be infeasible in practice. Eqs. (32)–(34) are evaluated many times during the actuation layout optimization [see section "Actuation Layout Optimization", Eqs. (15)–(19)]. For this reason, to increase computation speed, the buckling constraints in Eq. (33) are simplified by ignoring the effect of actuator length changes $\Delta \mathbf{l}$ on the element effective length. However, the effect of $\Delta \mathbf{l}$ on the element critical load is assessed in Eq. (16). In this way, the Hessian of the Lagrangian is $\mathbf{S}^T \mathbf{S}$, which is positive semidefinite where $\mathbf{S}$ is a full column rank rectangular matrix. For this reason, the problem stated in Eqs. (32)–(34) can be solved efficiently using interior-point method (IPM).

The actuator length changes $\Delta \mathbf{l}$ obtained as a solution of the problem stated in Eqs. (32)–(34) is approximate and therefore might not be able to cause an effective change of forces $\Delta \mathbf{f}^c$ and shape $\Delta \mathbf{d}^c$ through ϕ, which are close enough to $\Delta \mathbf{f}^t$ and $\Delta \mathbf{d}^t$. The Newton-Raphson scheme (Lax et al. 1972) is employed to iterate to convergence, which is achieved when $\|\Delta \mathbf{f}^c - \Delta \mathbf{f}^{c'}\|_2^2$ and
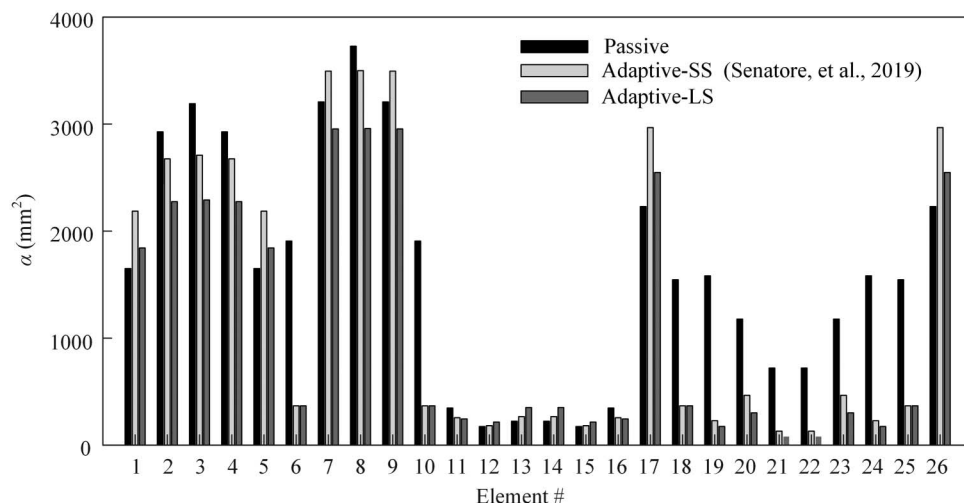

Fig. 5. Element cross-sectional area.

Table 2. Embodied energy savings

Nodal shift bound relative to $\mathbf{d}^{\text{input}}$ (mm)	Embodied energy savings with respect to adaptive-SS (%)	Embodied energy savings with respect to passive (%)
0	0	22.6
50	5.7	28.3
100	12.5	33.7
150	17.2	37.1

$\|\Delta\mathbf{d}^c - \Delta\mathbf{d}^{c'}\|_2^2$ is smaller than a set tolerance, where $\Delta\mathbf{f}^{c'}$ and $\Delta\mathbf{d}^{c'}$ are the change of forces and shape respectively at next iteration. The process can be summarized in the following steps:

1. In the first iteration internal forces $\mathbf{f}^c$ and shape $\mathbf{d}^c$ are set to $\mathbf{f}^0$ and $\mathbf{d}^0$, which are the forces and shapes caused by the external load without control (see section "Actuation Layout Optimization").
2. Shape and force influence matrices are computed using the current shape $\mathbf{d}^c$.
3. The actuator length change $\Delta\mathbf{l}$ is then obtained as the solution to the optimization problem stated in Eqs. (32)–(34).
4. Effective change of forces $\Delta\mathbf{f}^c$ and shape $\Delta\mathbf{d}^c$ caused by $\Delta\mathbf{l}$ are computed via ϕ.
5. If convergence is achieved, the process ends.
6. If convergence is not achieved, repeat from Step 2. The current values of $\mathbf{f}^c$ and $\mathbf{d}^c$ are set to $\mathbf{f}^c + \Delta\mathbf{f}^c$ and $\mathbf{d}^c + \Delta\mathbf{d}^c$, the target $\Delta\mathbf{f}^t$ and $\Delta\mathbf{d}^t$ are updated as $\Delta\mathbf{f}^t := \mathbf{f}^t - \mathbf{f}^c$ and $\Delta\mathbf{d}^t := \mathbf{d}^t - \mathbf{d}^c$, respectively.

The process is carried out for all n^p load cases. Algorithm 2 gives the pseudocode of the process to compute control commands given target shapes and an actuator layout.
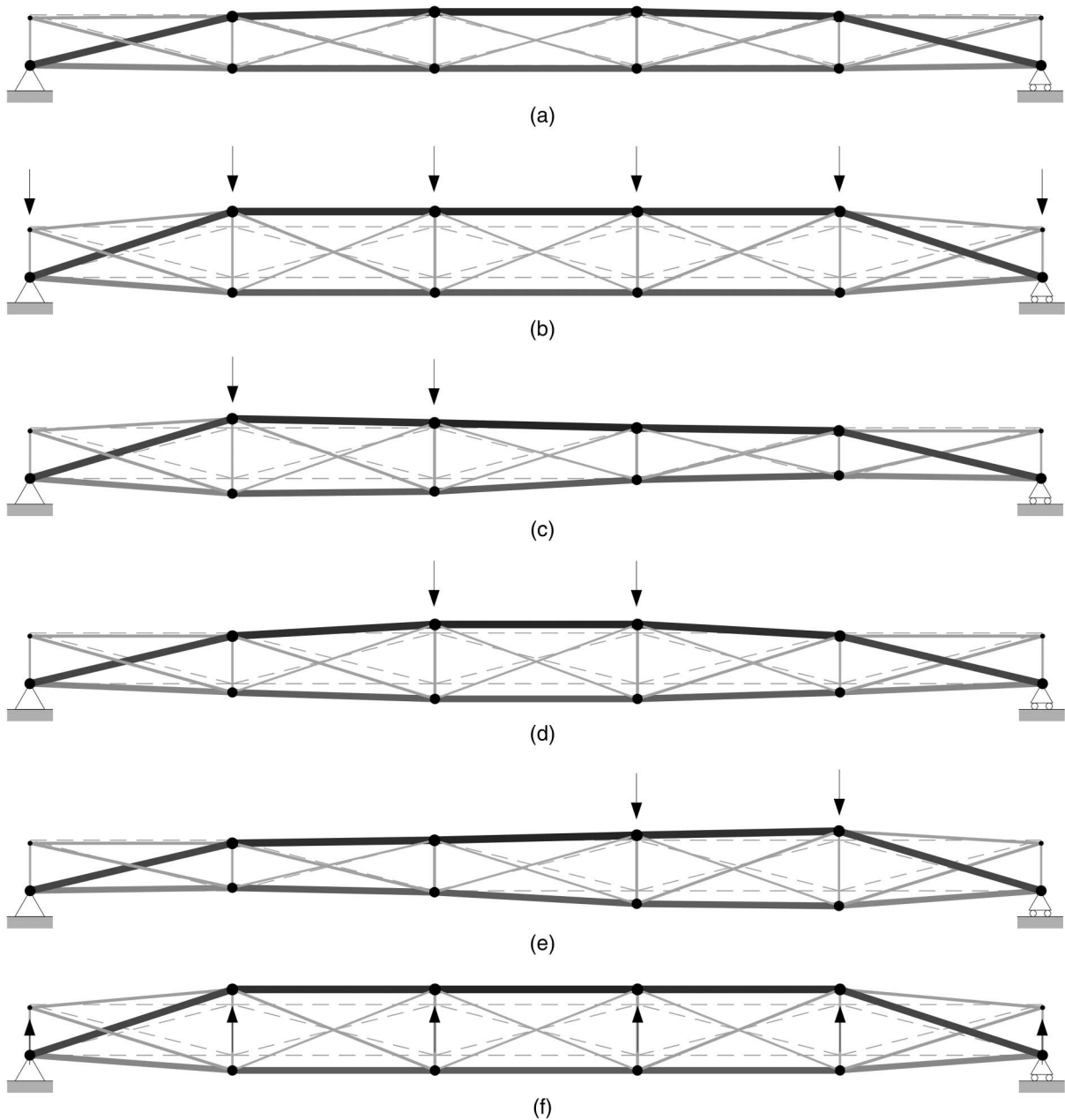

Fig. 6. Target shapes: (a) LC0, $\mathbf{d}_0^t$; (b) LC1, $\mathbf{d}_1^t$; (c) LC2, $\mathbf{d}_2^t$; (d) LC0, $\mathbf{d}_3^t$; (e) LC0, $\mathbf{d}_4^t$; and (f) LC0, $\mathbf{d}_5^t$.

Algorithm 2. Pseudocode of control command computation ϕ^{-1}

1	set as starting point $\mathbf{d}^0$, $\mathbf{f}^0$ and $\mathbf{l}^0$; the uncontrolled state under external loads
2	set starting point $\Delta\mathbf{d}^c\leftarrow0$, $\Delta\mathbf{f}^c\leftarrow0$
3	set current $\mathbf{d}^c\leftarrow\mathbf{d}^0$ and $\mathbf{f}^c\leftarrow\mathbf{f}^0$
3	**while** true do
5	set target $\Delta\mathbf{f}^t:=\mathbf{f}^t-\mathbf{f}^c$ and $\Delta\mathbf{d}^t:=\mathbf{d}^t-\mathbf{d}^c$
6	compute $\mathbf{S}_d$ and $\mathbf{S}_f$ through Eqs. (29) and (30)
7	obtain $\Delta\mathbf{l}$ through Eqs. (32) and (33)
8	compute $\Delta\mathbf{f}^{c'}$, $\Delta\mathbf{d}^{c'}$ through ϕ (Sec. 3)
14	**if** $\|\Delta\mathbf{f}^c-\Delta\mathbf{f}^{c'}\|_2^2<tol$ and $\|\Delta\mathbf{d}^c-\Delta\mathbf{d}^{c'}\|_2^2 < tol$ **then break**
	set $\mathbf{d}^c=\mathbf{d}^c+\Delta\mathbf{d}^{c'}$ and $\mathbf{f}^c=\mathbf{f}^c+\Delta\mathbf{f}^{c'}$
15	**end while**

Case Study

A roof structure, shown in Fig. 2, made of planar trusses is taken as a case study. Each truss has a span of 10 m, a span-to-depth ratio of 20:1 and it is assumed to support 2 m of cover in the out-of-plane direction. It is assumed that lateral stability is provided by other means. The topology and support conditions are indicated in Fig. 3(a). Node and element numbering is given in Figs. 3(b–d).

The structure is divided into six bays and consists of 26 elements. There are 24 degrees of freedom (12 nodes), of which three are fixed and hence the degree of static indeterminacy is 5. Note that the shape shown in Fig. 3(a) is the initial shape $\mathbf{d}^{input}$ defined in section "Shape and Internal Load-Path Optimization." The elements are made of structural steel (S355), with a Young's modulus of 210 GPa and a density of 7,850 kg/m³. To convert material mass into embodied energy, it is assumed the elements are made of primary steel without recycled contents with a material energy intensity (MEI) of 35 MJ/kg (Hammond and Jones 2008). The cross-bracing elements are assumed to slide freely. All elements have a cylindrical hollow section with a wall thickness set to 10% of the external diameter.

The structure is designed to support permanent and live load (Fig. 4). The permanent load consists of self-weight (SW) and a dead load (DL), which is applied on the top chord nodes as a
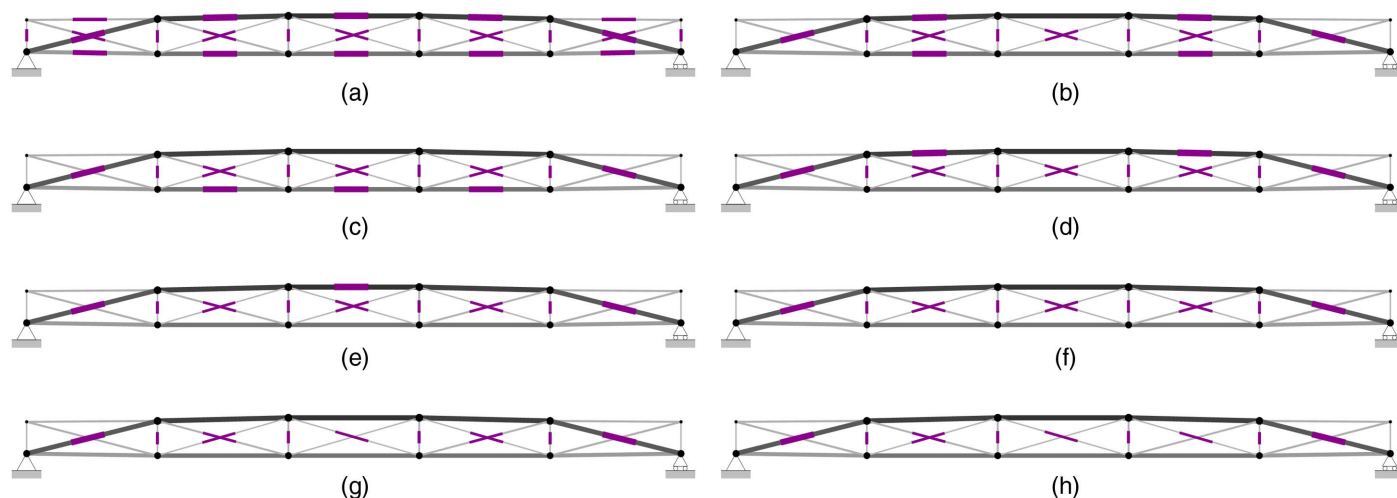

Fig. 7. Optimal actuator layouts for 26, 16, 15, 14, 13, 12, 11, and 10 actuators: (a) 26 actuators (all elements); (b) 16 actuators; (c) 15 actuators; (d) 14 actuators; (e) 13 actuators; (f) 12 actuators; (g) 11 actuators; and (h) 10 actuators.

Table 3. Comparison of optimal actuator layouts for 26, 16, 15, 14, 13, 12, 11, and 10 actuators

n^{act}	Size of the search domain	$1-Q$ Eq. (15)	Norm of shape discrepancy (mm)	Max shape discrepancy (mm)	Norm of internal load-path discrepancy (kN)	Max demand/capacity ratio
26	1	1.26×10^{-5}	1.97	1.45	34.04	0.95
16	5.3×10^6	2.44×10^{-5}	3.23	1.32	38.31	0.98
15	7.7×10^6	2.96×10^{-5}	3.65	1.51	37.13	0.98
14	9.6×10^6	5.45×10^{-5}	4.20	1.63	36.71	0.98
13	10.4×10^6	1.04×10^{-4}	6.87	2.34	35.32	0.98
12	9.6×10^6	1.15×10^{-4}	113.32	76.30	29.56	0.97
11	7.7×10^6	1.52×10^{-4}	174.23	113.00	41.55	15.64*
10	5.3×10^6	1.81×10^{-4}	239.51	156.78	44.23	21.20*

Note: The asterisk highlights Max demand/capacity ratios that are greater than one.
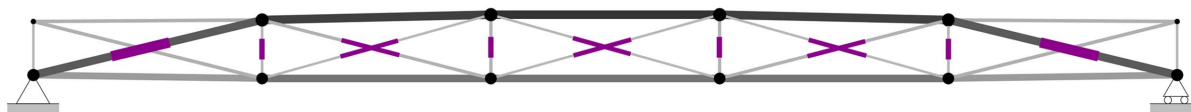

Fig. 8. Optimal actuator layout for 12 actuators.

distributed load of magnitude 500 kg/m². There are three cases for the live load (LL): LL1 is a uniformly distributed load with a magnitude 75% of DL; LL2 is a moving load with a magnitude 75% of DL applied on each bay in turn (LL2a to LL2c); and LL3 is a uniformly distributed uplift load with a magnitude 150% of DL. Table 1 summarizes all load combinations considered in this case study.

During geometry optimization χ (see section "Shape and Internal Load-Path Optimization"), all nodes except the supports are allowed to shift vertically within a range of ± 150 mm with respect to the initial geometry $\mathbf{d}^{\mathrm{input}}$. The element radius lower bound is set to 5 mm. There are 482 design variables entries; 26 are the cross-sectional areas α, 156 (26 entries × 6 load cases) the target internal forces $\mathbf{f}^t$, 156 entries (26 entries × 6 load cases) the noncontrolled internal forces under live load, and 144 (24 entries × 6 load cases) the nodal positions $\mathbf{d}^t$. Convergence is achieved after 16 iterations within 22 s on an Intel Core i7, 3.60 GHz.

The embodied energy of the adaptive design is benchmarked against the following: (1) an adaptive structure designed without
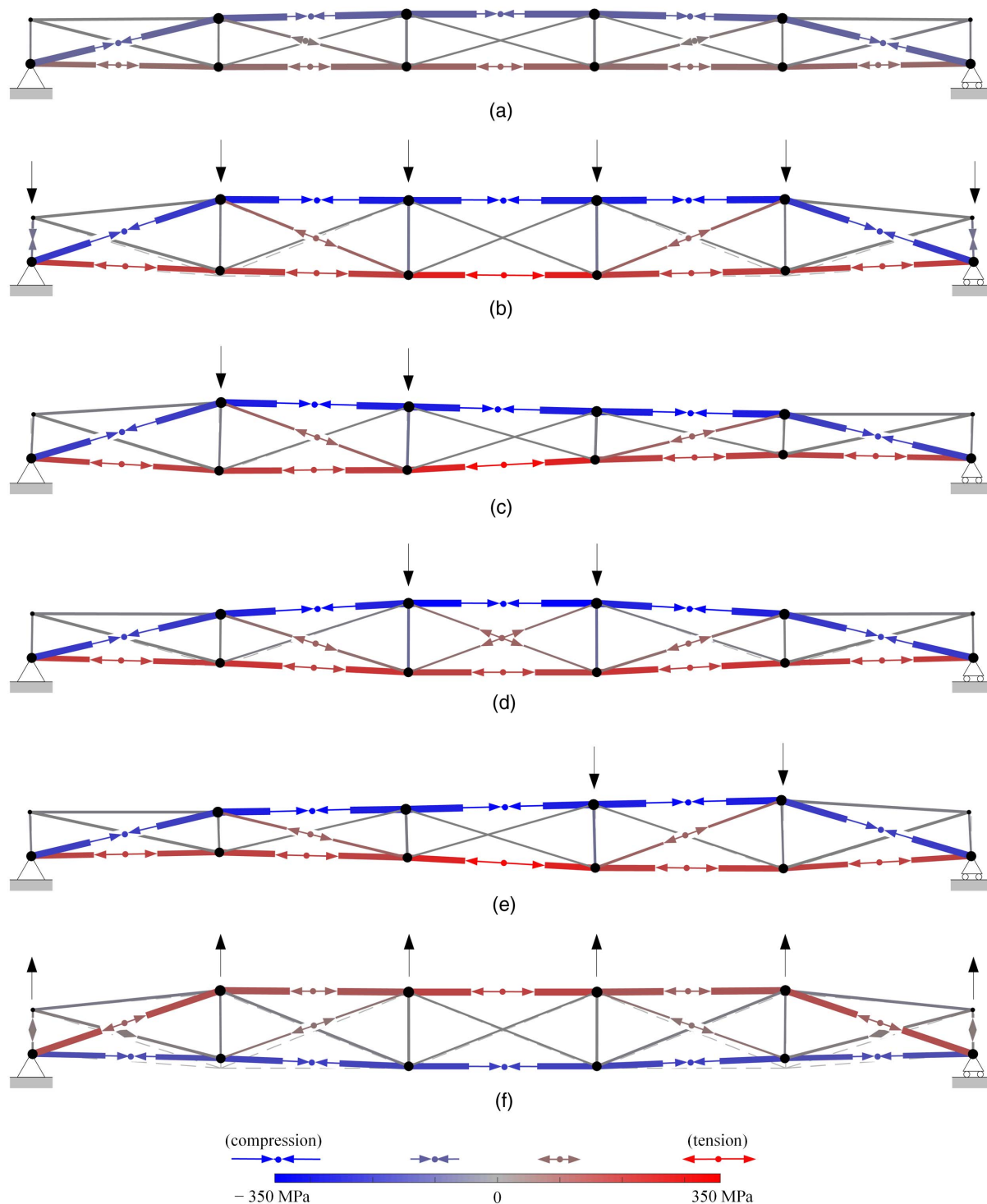

Fig. 9. Controlled shapes and element stress: (a) permanent load case; (b) first load case; (c) second load case; (d) third load case; (e) fourth load case; and (f) fifth load case.
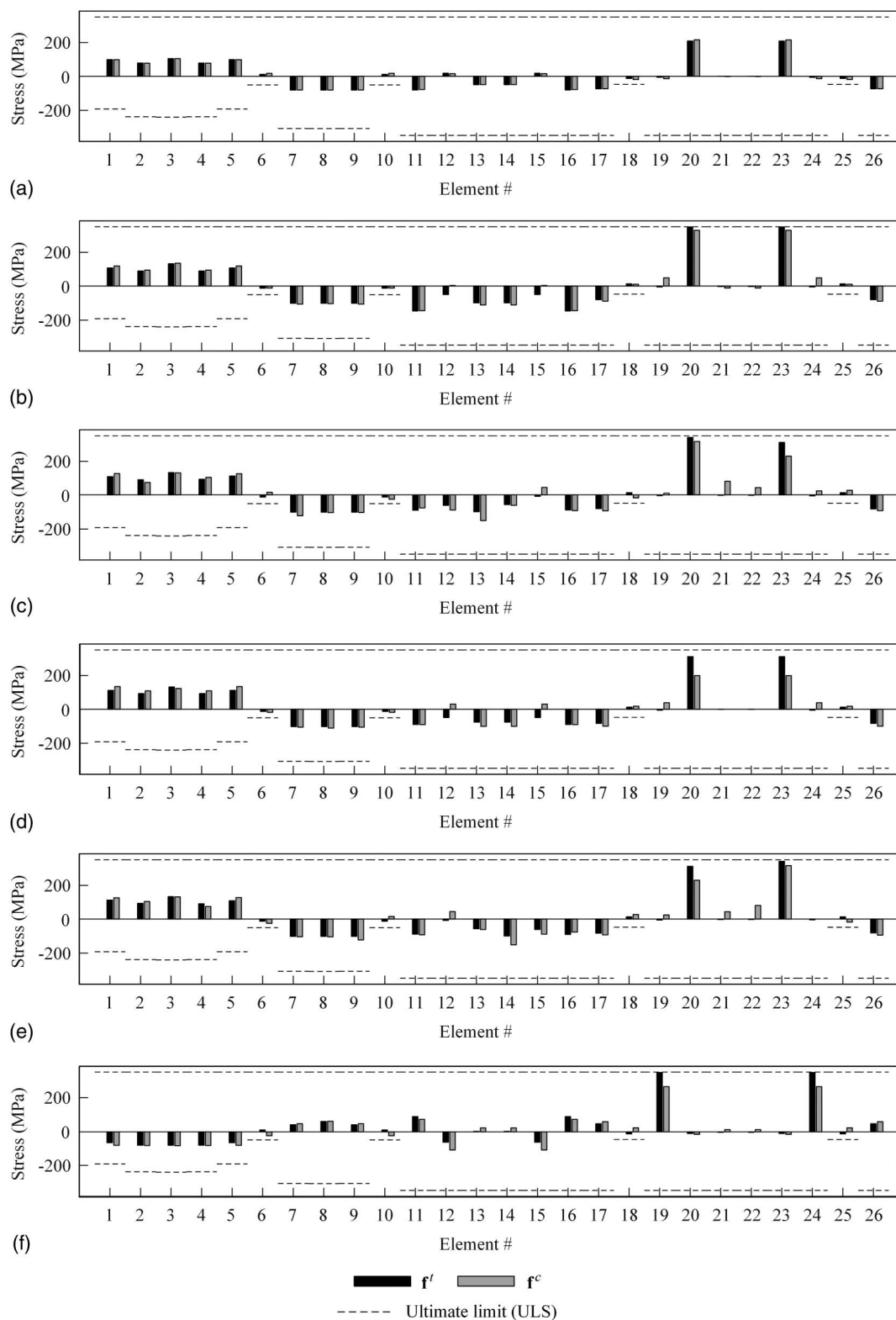
Fig. 10. Optimal and controlled element stress: (a) permanent load case; (b) first load case; (c) second load case; (d) third load case; (e) fourth load case; and (f) fifth load case.

considering large shape changes, i.e., excluding $\Delta\mathbf{d}$ from the design variables (Senatore et al. 2019); (2) a passive structure with identical topology that is weight-optimized using the same optimization for the first part but adding serviceability constraints so that no adaptation is necessary to satisfy both ULS and SLS constraints. The passive structure is designed considering an SLS defined by

the maximum nodal displacement of span divided by 360. Fig. 5 shows a comparison of the cross-sectional area between the three configurations. In general, employing large shape changes (adaptive-LS) yields smaller cross-sectional areas compared to an adaptive structure limited to small shape changes (adaptive-SS) as well as a passive one.

Table 4. Maximum element demand over capacity ratio without control

Load case	Max demand/capacity ratio excluding load factors	Max demand/capacity ratio including load factors	Element number
LC0 (permanent load case)	0.95	1.32	6, 10
LC1	0.97	1.41	6, 10
LC2	0.96	1.39	6
LC3	0.97	1.40	6, 10
LC4	0.96	1.39	10
LC5	0.76	1.17	18, 25

The embodied energy savings with respect to adaptive-SS and passive design are 17.2% and 37.1%, respectively. Table 2 gives the embodied energy savings with respect to the passive structure for different shape change bounds. The case where the nodal shifts are zero is identical with adaptive-SS (Senatore et al. 2019). As expected, larger shape changes result into larger embodied energy savings.

Fig. 6 shows the target shapes, the element diameter is indicated by line thickness variation and color shading (a darker shade of grey corresponds to a larger cross-sectional area). It can be observed that the structure increases its depth in proximity of the live load. Intuitively, an increase of depth helps to resist better the bending moment caused by the external load if the truss is thought of as a continuous beam. Shape optimization is not carried out for the adaptive-SS and passive structure. In these cases, the target shape is defined by the displacement limit with respect to the initial position of the controlled degrees of freedom.

The optimal actuator layout to control the structure into the target shapes and internal forces is obtained for n^{act} number of active elements. Generally, a low number of active elements is desired to reduce cost and control complexity. In addition, from Eq. (17), the size of the search space reaches a maximum when the number of actuators are one-half of the total number of elements. However, below a certain number of actuators, controllability cannot be achieved. The minimum number of actuators can be determined by running the actuator layout search to convergence for a decreasing number of active elements. Once the temperature level T reaches its lowest point, a new cycle starts by resetting T. Each succeeding cycle takes the final actuator layout of the preceding cycle as the initial candidate solution. The search process is stopped if (1) no improvement of the solution is achieved, or (2) no feasible solution has been obtained. In this case study, the search for an optimal actuator layout is repeated for all elements (26 total) set as active and then 16, 15, 14, 13, 12, 11, and 10 actuators. In each cycle of the constrained simulated annealing optimization there are $n^{temp} = 20$ temperature levels T, each containing $n^{rep} = 100$ evaluations of the objective and constraint functions.

Fig. 7 shows the optimal actuator layouts and Table 3 gives metrics related to all the cases considered in this study. In general, the solution is symmetrical with respect to the vertical axis at midspan, despite symmetry has not been explicitly enforced. The higher the number of actuators, the closer the controlled shapes match
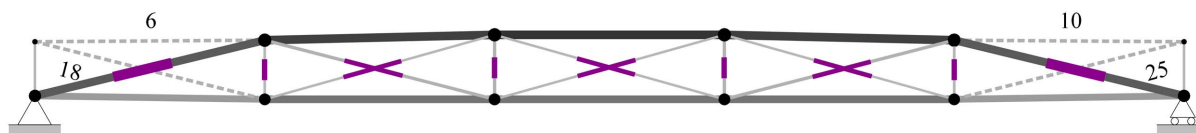
the optimal shapes. Solution feasibility is defined as the maximum element demand over capacity ratio after control for each actuator layout. For example, when the number of actuators is 11, the maximum element demand over capacity ratio is above 1, hence ULS is not respected. For any number of actuators less than 12, no feasible solution has been found.

Using the proposed heuristics based on the actuator control efficacy defined in section "Actuation Layout Optimization," optimal actuator layouts have been obtained after a number of evaluations that is relatively low. For example, when the layout is made of 12 actuators, convergence has been achieved after 13,667 evaluations (average of 10 runs) within an average time of 35 min on an Intel Core i7, 3.60 GHz. Using the same computer, when the problem is solved without heuristics, convergence is achieved after 45,102 evaluations within an average time of 142 min. A full enumeration requires 9.6×10^6 evaluations, which take approximately 15 days.

Because 12 is the minimum number of actuators to obtain feasible shape control, a more detailed analysis of this case is presented in the following. For clarity, this actuator layout is shown again in Fig. 8. Fig. 9 shows the controlled shapes with element stress mapped onto the geometry. The target shapes (Fig. 6) are represented as dashed lines for comparison. In general, controlled shapes match with target shapes. A discrepancy can be appreciated visually only for the fifth load case [Fig. 9(f)]. A difference between optimal and controlled shape is expected because not all the elements can change their lengths. The optimal shapes are obtained without considering geometric compatibility hence they could only be matched through control if all the elements are active. The internal forces are redirected predominantly toward the bottom chord (Elements $1-5$) for tension and through an arch-like structure consisting of Elements 17, 7, 8, 9, and 26 for compression. The maximum actuator extension is 334 mm for Elements 12 and 15 under load case (LC)1. The maximum actuator contraction is 61 mm for Elements 12 and 15 under LC2 and LC4, respectively.

Fig. 10 shows the bar charts of the target $\mathbf{f}^t$ (black) and controlled $\mathbf{f}^c$ (grey) internal forces for all load cases. Element capacity (ULS) is shown by a horizontal line. The controlled forces (grey bars) are generally in good agreement with the target forces (black bars). Elements 20 and 23 are highly stressed due to their small cross-sectional area (256 mm²), which is less than 10% that of Elements 7, 8, and 9 (2,940 mm²). However, ULS criteria are satisfied for all load cases. Maximum actuator forces are 137.1 kN in tension for Elements 20 and 23, and 252.4 kN in compression for Elements 17 and 26.

Table 4 indicates the maximum element demand over capacity ratio for the internal forces $\mathbf{f}_0$ in case no shape control is performed and $\mathbf{p}_j$ is applied on the target shape under permanent load $\mathbf{d}_0^t$. As discussed in section "Shape and Internal Load-Path Optimization", $\mathbf{f}^0$ are the internal forces in the event of control system failure (or power outage) and simultaneous occurrence of the design load $\mathbf{p}_j$. In this scenario, only four elements (6, 10, 18, and 25), which are indicated by dashed lines in Fig. 11, fail due to buckling without causing global failure of the structure. For this reason, $\mathbf{p}_j^0$ in Eq. (6) was reduced by excluding the load factors. This means that it is accepted that the active system contributes to satisfy ULS

Fig. 11. Elements with maximum demand over capacity ratios under no control.

requirements because in case of control system failure the structure does not collapse.

Discussion

For civil structures, even if the load has a very low occurrence probability, a failure might be unacceptable. For this reason, a fail-safe measure is often deemed as necessary. If optimization of geometry and internal load-path optimization (χ) is carried out without including the fail-safe measure defined in Eq. (6) the embodied energy savings increase to 25% (from 17%) and 43% (from 37%) with respect to adaptive-SS and the passive configuration.

The fail-safe measure can be also relaxed by setting $\mathbf{p}^0$ to a lower intensity with respect to the design load $\mathbf{p}$. This means that the structure is designed so that the active system contributes to satisfying ULS requirements. For the case study presented in this paper, $\mathbf{p}^0$ was obtained from the design load $\mathbf{p}$ by omitting the load factors. Given that the design load is usually a rare event of extreme intensity, a reduced load factor for the fail-safe measure means that the structure is able to resist passively to loading events of lower intensity but that might occur more frequently.

The geometry and internal load-path optimization χ formulated in section "Shape and Internal Load-Path Optimization" is nonconvex because the nodal coordinates are part of the design variables and due to the buckling constraints. For this reason, optimization though sequential quadratic programming may result in a local minimum. He and Gilbert (2015) have shown that imposing upper and lower limits on the change of node positions with respect to the initial shape is effective to exclude undesirable local optima such as those associated with significantly different shapes (e.g., node reversal, node/element merging). In the context of shape adaptation such solutions are not of interest, as shape control would be impractical. Therefore, definition of limits and the initial configuration for the nodal position is critical. The quality of the solution can be evaluated through comparison against other methods, for example those based on linearization (Pedersen 1973; Schwarz et al. 2018) or those that include analytical sensitivity (Nocedal and Wright 1999) (e.g., Jacobian and Hessian).

Global optimality of the solution produced by the actuator placement optimization given in the section "Actuation Layout Optimization" can neither be guaranteed nor verified due to the large size of the search domain. For this reason, the actuator layouts obtained with this method are local minima or could be considered as optimally-directed solutions.

Conclusions

A new method to design adaptive structures is presented in this article. The primary contribution of this work is the use of large-shape changes to counteract the effect of external loads so that the design is not governed by peak loads. This is because large-shape changes allow the structure to effectively redirect the internal forces, thus minimizing the maximum stress governing the design. Simulations have shown that this method produces efficient structures. For a simply supported truss of 10 m span and 0.5 m height, up to 17% and 37% embodied energy savings are gained compared to an equivalent adaptive structure that is designed and controlled through small shape changes and to a weight-optimized passive structure, respectively.

Optimal actuator placement has been formulated as a combination of constrained simulated annealing and the nonlinear force method. This process produces appropriate actuator layout and control commands to control the structure into required shapes. This is

a challenging task due to the combinatorial nature of the actuator placement process, which in this case includes geometric nonlinearity. A heuristic for neighbor solution generation based on an actuator control efficacy measure has been developed to help exploring the large search space. The heuristic has significantly improved convergence, which is important for structures with complex topologies that are made many elements. Simulations have shown that this method successfully produces actuator layouts to control the shape and internal forces as required with a low number of actuators relative to the total number of structural elements.

Future work will include whole-life energy appraisals comprising the energy embodied in the material and the operational energy for structural adaptation. Also subject of future investigation are (1) case studies of structures with more complex topologies to generalize the conclusions reached in this work, and (2) experimental testing to validate the feasibility of this method when applied to the design and control of real structures.

Acknowledgments

Notation

The following symbols are used in this paper:

$\mathbf{A}$ = equilibrium matrix;

$\mathbf{B}$ = compatibility matrix;

$\mathbf{d}^c$ = controlled shape;

$\mathbf{d}^t$ = optimal (target) shape;

$\mathbf{d}^t_j$ = optimal (target) shape under the jth load case;

$\mathbf{d}^{input}$ = initial geometry;

$\mathbf{d}^0$ = deformed shape (no control) computed from $\mathbf{d}^t_0$;

E = Young's modulus;

$\mathbf{f}$ = internal forces;

$\mathbf{f}^c$ = controlled internal forces;

$\mathbf{f}^t$ = optimal (target) forces;

$\mathbf{f}^t_j$ = optimal (target) forces in equilibrium with the jth load case;

$\mathbf{f}^0$ = internal forces (no control) computed on $\mathbf{d}^t_0$;

$\mathbf{G}$ = flexibility matrix;

g = material energy intensity (MEI);

I = element second moment of area;

i = ith element;

J = objective function in actuator layout optimization;

j = jth load case;

$\mathbf{l}$ = element length;

n^{act} = number of actuators;

n^{cd} = number of controlled degrees of freedom;

n^d = number of degrees of freedom;

n^e = number of elements;

n^n = number of nodes;

n^p = number of load cases;

n^{rep} = number of repetitions;

n^{temp} = number of temperature levels;

$O^{\mathbf{y}}$ = probability of acceptance of candidate actuator layout $\mathbf{y}$;

O^{γ} = probability of acceptance of penalty factor γ;

$\mathbf{P}$ = element control efficacy;

$\mathbf{p}$ = external load;

Q = Tanimoto similarity index;

r = degree of static indeterminacy;

$\mathbf{S}_d$ = shape influence matrix;

$\mathbf{S}_f$ = force influence matrix;

$\mathbf{S}_d^*$ = reduced shape influence matrix;

$\mathbf{S}_f^*$ = reduced force influence matrix;

T = temperature level;

$\mathbf{W}_s$ = states of self-stress;

$\mathbf{x}$ = design variable vector: $\boldsymbol{\alpha}$, $\mathbf{f}$, $\mathbf{d}^t$;

$\mathbf{y}$ = actuator positions (actuator layout);

$\boldsymbol{\alpha}$ = element cross-sectional areas;

γ = penalty factor;

$\Delta\mathbf{d}^c$ = controlled shape change;

$\Delta\mathbf{f}$ = change of internal forces;

$\Delta\mathbf{f}^c$ = controlled change of internal forces;

$\Delta\mathbf{f}^t$ = target (optimal) change of internal forces;

$\Delta\mathbf{l}$ = control commands (actuator length changes);

$\Delta\mathbf{l}^e$ = control commands when all elements are active;

ρ = material density;

σ^- = ultimate compressive stress;

ϕ = computation of internal forces and shape given control commands;

ϕ^{-1} = computation of control commands given target shape and internal forces; and

χ = mapping between external load and shapes.

References

Achtziger, W. 2007. "On simultaneous optimization of truss geometry and topology." *Struct. Multidiscip. Optim.* 33 (4–5): 285–304. https://doi.org/10.1007/s00158-006-0092-0.

Adam, B., and I. F. C. Smith. 2008. "Active tensegrity: A control framework for an adaptive civil-engineering structure." *Comput. Struct.* 86 (23–24): 2215–2223. https://doi.org/10.1016/j.compstruc.2008.05.006.

Akgün, Y., C. J. Gantes, W. Sobek, K. Korkmaz, and K. Kalochairetis. 2011. "A novel adaptive spatial scissor-hinge structural mechanism for convertible roofs." *Eng. Struct.* 33 (4): 1365–1376. https://doi.org/10.1016/j.engstruct.2011.01.014.

Arora, J., O. Elwakeil, and A. Chahande. 1995. "Global optimization methods for engineering applications: A review." *Struct. Optim.* 9 (3–4): 137–159. https://doi.org/10.1007/BF01743964.

Bajusz, D., A. Rácz, and K. Héberger. 2015. "Why is Tanimoto index an appropriate choice for fingerprint-based similarity calculations?" *J. Cheminf.* 7 (1): 1–20.

Barnes, M. 1977. "Form finding and analysis of tension space structures by dynamic relaxation." *Int. J. Space Struct.* 14 (2): 89–104. https://doi.org/10.1260/0266351991494722.

Begg, D., and X. Liu. 2000. "On simultaneous optimization of smart structures. II: Algorithms and examples." *Comput. Methods Appl. Mech. Eng.* 184 (1): 25–37. https://doi.org/10.1016/S0045-7825(99)00317-5.

Boogs, P., and J. Tolle. 1995. "Sequential quadratic programming." *Acta Numer.* 4 (1): 1–51.

Cerny, V. 1985. "A thermodynamic approach to the traveling salesman problem: An efficient simulation." *J. Optim. Theory Appl.* 45 (1): 41–51.

Connor, J. 2002. *Introduction to structural motion control.* Boston: Pearson Education.

Crisfield, M. 1981. "A fast incremental/iterative solution procedure that handles 'snap-through.'" *Comput. Struct.* 13 (1–3): 55–62. https://doi.org/10.1016/0045-7949(81)90108-5.

Day, A. 1965. "An introduction to dynamic relaxation." *Engineer* 219 (5688): 218–221.

Descamps, B. 2014. *Computational design of lightweight structures: Form finding and optimization.* London: Wiley.

Doan, A., J. Madhavan, P. Domingos, and A. Halevy. 2004. "Ontology matching: A machine learning approach." In *Handbook on ontologies*, 385–403. Berlin: Springer.

EEA (European Environment Agency). 2010. *Material resources and waste: The European environment: State and outlook.* Luxembourg: Publications Office of the European Union.

Gantes, C., J. Connor, R. Logcher, and Y. Rosenfeld. 1989. "Structural analysis and design of deployable structures." *Comput. Struct.* 32 (3): 661–669. https://doi.org/10.1016/0045-7949(89)90354-4.

Gil, L., and A. Andreu. 2001. "Shape and cross-section optimisation of a truss structure." *Comput. Struct.* 79 (7): 681–689. https://doi.org/10.1016/S0045-7949(00)00182-6.

Haftka, R. T. 1985. "Simultaneous analysis and design." *AIAA J.* 23 (7): 1099–1103. https://doi.org/10.2514/3.9043.

Hammond, G., and C. Jones. 2008. "Embodied energy and carbon in construction materials." *Proc. Inst. Civ. Eng. Ene.* 161 (2): 87–98. https://doi.org/10.1680/ener.2008.161.2.87.

He, L., and M. Gilbert. 2015. "Rationalization of trusses generated via layout optimization." *Struct. Multidiscip. Optim.* 52 (4): 677–694. https://doi.org/10.1007/s00158-015-1260-x.

Kirkpatrick, S., J. C. Gelatt, and M. Vecchi. 1983. "Optimization by simulated annealing." *Science* 220 (4598): 671–680. https://doi.org/10.1126/science.220.4598.671.

Kobori, T., and S. Kamagata. 1991. "Dynamic intelligent buildings-active seismic response control." In *Intelligent structures*, 279–282. Milton Park, Abingdon: Taylor & Francis Group.

Korkmaz, S., N. B. H. Ali, and I. Smith. 2012. "Configuration of control system for damage tolerance of a tensegrity bridge." *Adv. Eng. Inf.* 26 (1): 145–155. https://doi.org/10.1016/j.aei.2011.10.002.

Lax, P., S. Burstein, and A. Lax. 1972. *Calculus with applications and computing.* New York: Courant Institute of Mathematical Sciences, New York Univ.

Manning, R. 1991. "Optimum design of intelligent truss structures." In *Proc., 32nd Structures, Structural Dynamics, and Materials Conf.*, 528–533. Reston, VA: American Institute of Aeronautics and Astronautics.

Metropolis, N., A. Rosenbluth, A. Teller, and E. Teller. 1953. "Equation of state calculations by fast computing machines." *J. Chem. Phys.* 21 (6): 1087–1092.

Nakajima, K., N. Giron, M. Kohiyama, K. Watanabe, M. Yoshida, M. Yamanaka, S. Inaba, and O. Yoshida. 2012. "Seismic response analysis of a semi-active-controlled base-isolated building durinh the 2011 great east Japan earthquake." In *Proc., Int. Symp. on Engineering Lessons Learned from the 2011 Great East Japan Earthquake.*

Nocedal, J., and S. Wright. 1999. *Numerical optimization.* New York: Springer.

Onoda, J., and Y. Hanawa. 1992. "Actuator placement optimization by genetic and improved simulated annealing algorithms." *AIAA J.* 31 (6): 1167–1169. https://doi.org/10.2514/3.49057.

Patnaik, S., D. Hopkins, and G. Halford. 2004. *Integrated force method solution to indeterminate structural mechanics problems.* Washington, DC: National Aeronautics and Space Administration.

Pedersen, N., and A. Nielsen. 2003. "Optimization of practical trusses with constraints on eigenfrequencies, displacements, stresses, and buckling." *Struct. Multidiscip. Optim.* 25 (5–6): 436–445. https://doi.org/10.1007/s00158-003-0294-7.

Pedersen, P. 1973. "Optimal joint positions for space trusses." *J. Struct. Div.* 99 (12): 2459–2476.

Pellegrino, S. 2001. *Deployable structures.* New York: Springer.

Querin, O. 1997. "Evolutionary structural optimization: Stress based formulation and implementation." Ph.D. dissertation, Univ. of Sydney.

Reddy, G., and J. Cagan. 1995. "An improved shape annealing algorithm for truss topology generation." *ASME J. Mech. Des.* 117 (2): 315–321. https://doi.org/10.1115/1.2826141.

Reinhorn, A., T. R. M. Soong, and R. Lin. 1993. "Full-scale implementation of active control. II: Installation and performance." *J. Struct. Eng.*

119 (6): 1935–1960. https://doi.org/10.1061/(ASCE)0733-9445(1993)
119:6(1935).

Rhode-Barbarigos, L., C. Schulin, N. B. H. Ali, R. Motro, and I. F. Smith.
2012. "Mechanism-based approach for the deployment of a tensegrity-
ring module." *J. Struct. Eng.* 138 (4): 539–548. https://doi.org/10.1061
/(ASCE)ST.1943-541X.0000491.

Sauve, R. 1995. "Advances in dynamic relaxation techniques for nonlinear
finite element." *J. Pressure Vessel Technol.* 117 (2): 170–176. https://
doi.org/10.1115/1.2842106.

Schwarz, J., T. Chen, K. Shea, and T. Stanković. 2018. "Efficient size and
shape optimization of truss structures subject to stress and local buck-
ling constraints using sequential linear programming." *Struct. Multidis-
cip. Optim.* 58 (Jan): 171–184. https://doi.org/10.1007/s00158-017
-1885-z.

Senatore, G., P. Duffour, S. Hanna, F. Labbé, and P. Winslow. 2011. "Adap-
tive structures for whole-life energy savings." *J. Int. Assoc. Shell Spatial
Struct.* 52 (4): 233–240.

Senatore, G., P. Duffour, and P. Winslow. 2018a. "Energy and cost analysis
of adaptive structures: Case studies." *J. Struct. Eng.* 144 (8): 04018107.
https://doi.org/10.1061/(ASCE)ST.1943-541X.0002075.

Senatore, G., P. Duffour, and P. Winslow. 2018b. "Exploring the application
domain of adaptive structures." *Eng. Struct.* 167 (1): 608–628. https://
doi.org/10.1016/j.engstruct.2018.03.057.

Senatore, G., P. Duffour, and P. Winslow. 2019. "Synthesis of minimum
energy adaptive structures." *Struct. Multidiscip. Optim.* 60 (3): 849–877.
https://doi.org/10.1007/s00158-019-02224-8.

Senatore, G., P. Duffour, P. Winslow, and C. Wise. 2018c. "Shape control
and whole-life energy assessment of an "infinitely stiff." prototype
adaptive structure." *Smart Mater. Struct.* 27 (1): 015022. https://doi.org
/10.1088/1361-665X/aa8cb8.

Senatore, G., and D. Piker. 2015. "Interactive real-time physics: An intui-
tive approach to form-finding and structural analysis for design and
education." *Comput.-Aided Des.* 61 (Apr): 32–41. https://doi.org/10
.1016/j.cad.2014.02.007.

Shea, K., E. Fest, and I. Smith. 2002. "Developing intelligent tensegrity
structures with stochastic search." *Adv. Eng. Inf.* 16 (1): 21–40. https://
doi.org/10.1016/S1474-0346(02)00003-4.

Skelton, R., and C. Sultan. 1997. "Integrated design of controllable tensegr-
ity structures." *Adapt. Struct. Mater. Syst.* (1): 54: 27–35.

Sobek, W., and P. Teuffel. 2001. "Adaptive systems in architecture and
structural engineering." In Vol. 4330 of *Proc., Smart Structures and
Materials 2001: Smart Systems for Bridges, Structures, and Highways*,
36–45. Bellingham, WA: International Society for Optics and Photonics.

Soong, T. 1988. "Active structural control in civil engineering." *Eng. Struct.*
10 (2): 74–84. https://doi.org/10.1016/0141-0296(88)90033-8.

Soong, T., and G. Cimellaro. 2009. "Future directions in structural control."
Struct. Control Health Monit. 16 (7): 7–16.

Soong, T., and G. Manolis. 1987. "Active structures." *J. Struct. Eng.*
113 (11): 2290–2302. https://doi.org/10.1061/(ASCE)0733-9445(1987)
113:11(2290).

Spencer, Jr., B., and S. Nagarajaiah. 2003. "State of the art of structural
control." *J. Struct. Eng.* 129 (7): 845–856.

Straube, J. 2006. "Green building and sustainability." In *Building science
digests*. Westford, MA: Building Science Corporation.

Sychterz, A., and I. Smith. 2018. "Deployment and shape change of a ten-
segrity structure using path-planning and feedback control." *Front.
Built Environ.* 4: 45. https://doi.org/10.3389/fbuil.2018.00045.

Tanimoto, T. 1958. *An elementary mathematical theory of classification
and prediction*. New York: IBM.

Teuffel, P. 2004. "Entwerfen adaptiver strukturen." Ph.D. dissertation,
Fakultät Bau- und Umweltingenieurwissenschaften, Univ. of
Stuttgart–ILEK.

Veuve, N., S. Safei, and I. Smith. 2015. "Deployment of a tensegrity foot-
bridge." *J. Struct. Eng.* 141 (11): 04015021. https://doi.org/10.1061
/(ASCE)ST.1943-541X.0001260.

Wah, B., and T. Wang. 1999. "Constrained simulated annealing with ap-
plications in nonlinear continuous constrained global optimization." In
Proc., 11th Int. Conf. on Tools with Artificial Intelligence, 381–388.
New York: IEEE.

Wang, D., W. Zhang, and J. Jiang. 2002. "Truss shape optimization with
multiple displacement constraints." *Comput. Methods Appl. Mech. Eng.*
191 (33): 3597–3612. https://doi.org/10.1016/S0045-7825(02)00297-9.

Xu, X., and Y. Luo. 2009. "Non-linear displacement control of prestressed
cable structures." *J. Aerosp. Eng.* 223 (7): 1001–1007.

Yuan, X., X. Liang, and A. Li. 2016. "Shape and force control of pre-
stressed cable-strut structures based on nonlinear force method."
Adv. Struct. Eng. 19 (12): 1917–1926. https://doi.org/10.1177/13694
33216652411.